ELSEVIER

Journal of Electron Spectroscopy and Related Phenomena 69 (1994) 125–132

JOURNAL OF ELECTRON SPECTROSCOPY and Related Phenomena

Implementation of an efficient analytical approximation to the Voigt function for photoemission lineshape analysis☆

A.B. McLean*, C.E.J. Mitchell, D.M. Swanston

Department of Physics, Queen's University, Kingston, Ontario K7L 3N6, Canada

First received 24 September 1993; in final form 20 January 1994

Abstract

The Voigt function is used extensively in lineshape analysis of core-level photoemission spectra from non-metallic solids. It is often generated by numerically convoluting a Lorentzian spectral function with a Gaussian function which models the thermal and instrumental broadening. The convolution process is time consuming and the analysis of core-level photoemission data is usually the domain of high performance workstations or mainframe computers. However, a high accuracy analytical approximation has been found for the Voigt function and an implementation of this approximation is presented in this paper. It is demonstrated that the approximation brings lineshape analysis within the domain of the desktop computer.

Keywords: Accuracy; Approximation; Lineshape analysis; Novel; PC; Voigt

1. Introduction

Lineshape analysis of core-level photoemission energy distribution curves has matured into a standard analysis technique, which is performed to extract information about the chemical state and abundance of species on surfaces [1,2]. For a metal the core-level photoemission lineshape is asymmetric due to the creation of particle and hole-like excitations during the photoemission process [3]. The line profile also contains satellites at integer multiples of the plasmon energy due to the creation of collective excitations in the electron gas. For semiconductors and insulators, which have no occupied states at the Fermi level, the metallic Doniach Ŝunjić lineshape reduces to a Lorentzian [1]. Although they have not been studied in nearly as much detail, the lineshapes of some surface states on metal and semiconductor surfaces have also been shown to be well described by a Lorentzian function as long as the state is not in resonance with the bulk continuum [4–6].

To fully describe the photoemission spectra, the Lorentzian spectral function is convoluted with a Gaussian function, to simulate both the vibrational phonon broadening and the finite instrumental resolution of the electron spectrometer. This convolution produces a Voigt function [7]

$$V(X,Y) = \frac{Y}{\pi}\int_{-\infty}^{+\infty} \mathrm{d}z \, \frac{e^{-z^2}}{Y^2 + (X-z)^2} \qquad (1)$$

☆ Copies of the computer code referred to in this paper may be obtained from A.B. McLean by e-mail request to alastair@hecate. phy. queensu. ca.

* Corresponding author.

SSDI 0368-2048(94)02189-7

which has to be generated, scaled appropriately and added to an analytical function describing the secondary electron background. The generation of the Voigt function involves a numerical integration. This is the time limiting factor in most lineshape analysis. Consequently photoemission lineshape analysis is usually the domain of high performance workstations or mainframe computers and it is rarely performed on the computer that is used to collect the photoemission data. To circumvent this limitation, approximate methods have been developed for generating the Voigt function. One of these approximates the Voigt function with a linear combination of a Gaussian and a Lorentzian function [8]. The extraction of the Gaussian and Lorentzian linewidths from the parameters used in the approximation is performed using a look-up table. This method is still used in photoemission lineshape analysis [9]. More recently [10,11], an analytical approximation to the Voigt function has been made using four generalized Lorentzians in two variables. The Voigt function is expressed as

$$V(X,Y) = \sum_{i=1}^{4} \frac{C_i(Y - A_i) + D_i(X - B_i)}{(Y - A_i)^2 + (X - B_i)^2} \tag{2}$$

where $A_i \rightarrow D_i$ are a set of 16 constants. The values of the constants used to generate the Voigt approximation are given in Table 1. As pointed out previously [12], the source paper [11] contained some typographical errors and the correct parameters are given here for reference. As discussed in Ref. 11 this approximation is more accurate than the linear combination of a Gaussian and a Lorentzian function and no additional parameters are introduced in the approximation, so a look-up table is not required.

In this paper we present an implementation of this approximation that can easily be incorporated into a photoemission lineshape analysis program. To generate the photoemission lineshape $I(\varepsilon)$ we convolute a Lorentzian spectral function with a normalized Gaussian broadening function

$$I(\varepsilon) = \int_{-\infty}^{+\infty} G(\varepsilon')L(\varepsilon - \varepsilon')\mathrm{d}\varepsilon' \tag{3}$$

where the Lorentzian spectral function

$$L(\varepsilon) = \frac{a_L}{1 + 4(\varepsilon/\gamma_L)^2} \tag{4}$$

has an amplitude a_L and a FWHM of γ_L and the Gaussian broadening function

$$G(\varepsilon) = \frac{1}{\sigma\sqrt{2\pi}} \exp(-\varepsilon^2/2\sigma^2) \tag{5}$$

has a standard deviation of σ. This integral can readily be expressed in terms of the Voigt function, as defined above, as follows

$$I(\varepsilon) = \frac{a_L\gamma_L}{2\sigma}\sqrt{\frac{\pi}{2}}\, V(X,Y) \tag{6}$$

by making some simple transformations. The input parameters X and Y become

$$X = \frac{\varepsilon}{\sigma\sqrt{2}} \tag{7}$$

and

$$Y = \frac{\gamma_L}{\sigma 2\sqrt{2}} \tag{8}$$

respectively. (Note that these expressions are different from the ones listed in Ref. 12 which contained several typographical errors that were corrected in a later paper by the same author [13].) More usefully, these equations can be expressed in terms of the FWHM Gaussian linewidth (γ_G) using the identity that $\gamma_G = 2\sigma\sqrt{2\ln 2}$. Then

$$I(\varepsilon) = \frac{\gamma_L}{\gamma_G} a_L \sqrt{\pi(\ln 2)}\, V(X,Y) \tag{9}$$

$$X = \frac{2\sqrt{\ln 2}}{\gamma_G}\varepsilon \tag{10}$$

Table 1
Parameters used to generate the numerical approximation to the Voigt function

i	A_i	B_i	C_i	D_i
1	−1.2150	1.2359	−0.3085	0.0210
2	−1.3509	0.3786	0.5906	−1.1858
3	−1.2150	−1.2359	−0.3085	−0.0210
4	−1.3509	−0.3786	0.5906	1.1858

and

$$Y = \frac{\gamma_L}{\gamma_G}\sqrt{\ln 2} \tag{11}$$

2. Implementation

To utilize the Voigt function approximation in a non-linear least-squares lineshape analysis program, the parameter derivatives have to be supplied. One advantage of using an analytical approximation is that the derivatives can be evaluated analytically, and in this section the parameter derivatives will be derived. To avoid introducing another level of indices, it will be assumed that the photoemission energy distribution comprises only one Voigt function with no secondary electron background. However, the implementation that is presented in Appendix B assumes that the photoemission energy distribution curve does contain multiple Voigts, as it would in practice.

If the Voigt centre is displaced by ε_0, the photoemission energy distribution $I(\varepsilon)$ can be written as $I(\varepsilon; a_L, \varepsilon_0, \gamma_L, \gamma_G)$ and the four parameter derivatives are

$$\frac{\partial I}{\partial a_L} = \frac{C}{a_L} V(X,Y) \tag{12}$$

$$\frac{\partial I}{\partial \varepsilon_0} = -C\frac{(2\sqrt{\ln 2})}{\gamma_G}\frac{\partial V}{\partial X} \tag{13}$$

$$\frac{\partial I}{\partial \gamma_L} = C\left(\frac{V(X,Y)}{\gamma_L} + \frac{\partial V}{\partial Y}\frac{\sqrt{\ln 2}}{\gamma_G}\right) \tag{14}$$

and

$$\frac{\partial I}{\partial \gamma_G} = -\frac{C}{\gamma_G}\left(V(X,Y) + \frac{\sqrt{\ln 2}}{\gamma_G}\left[2(\varepsilon - \varepsilon_0)\frac{\partial V}{\partial X} + \gamma_L\frac{\partial V}{\partial Y}\right]\right) \tag{15}$$

where $C = \gamma_L a_L \sqrt{\pi(\ln 2)}/\gamma_G$. The partial derivatives of the Voigt function can be expressed as

$$\frac{\partial V}{\partial X} = \sum_{i=1}^{4}\left(D_i - \frac{2(X - B_i)\alpha_i}{\beta_i}\right)\beta_i^{-1} \tag{16}$$

and

$$\frac{\partial V}{\partial Y} = \sum_{i=1}^{4}\left(C_i - \frac{2(Y - A_i)\alpha_i}{\beta_i}\right)\beta_i^{-1} \tag{17}$$

where

$$\alpha_i = C_i(Y - A_i) + D_i(X - B_i) \tag{18}$$

and

$$\beta_i = (Y - A_i)^2 + (X - B_i)^2 \tag{19}$$

An ANSI C implementation of the Voigt approximation is presented in Appendix A. This implementation can be used to generate the Voigt photoemission energy distribution $I(\varepsilon)$. An implementation of the approximation that also evaluates the parameter derivatives is presented in Appendix B. This function is written so that it can be called from the *mrqmin* routine found in Numerical Recipes in C [14]. *mrqmin* is an ANSI C implementation of the Levenberg–Marquardt method [15].

The lineshape analysis described in the remainder of this paper was performed with a software package called CONVERGENCE which is implemented in C++ and runs on a NeXT computer within a standard UNIX terminal window. The non-linear, least-squares minimization was performed using an implementation of the Levenberg–Marquardt method [15] and the implementation of the Voigt function approximation is identical to the one that is listed in Appendix B, apart from the incorporation of code to model the secondary electron background.

3. Efficiency

To test the efficiency of the analytical Voigt function approximation, a synthetic Si2p core-level

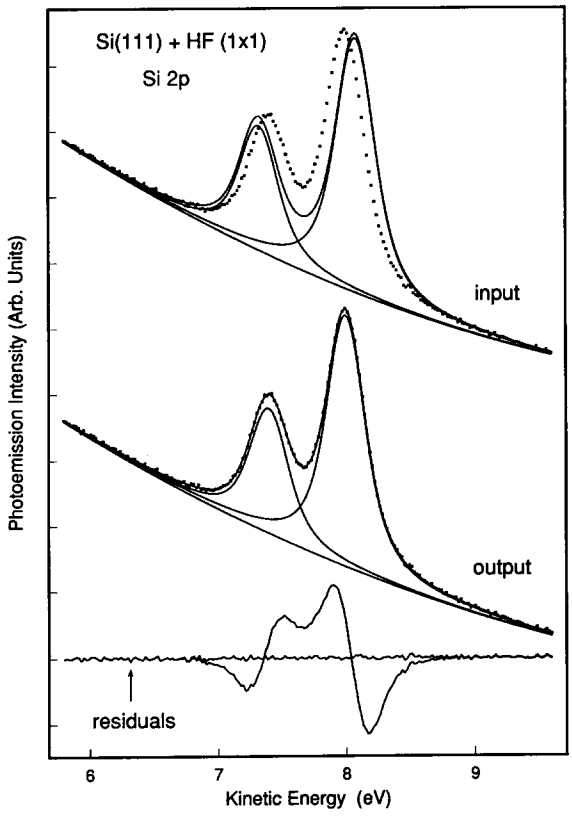

Fig. 1. The dots represent a synthetically generated Si2p core level comprising one Voigt doublet, which is spin–orbit split by 0.6 eV, superimposed on a quadratic secondary electron background. The parameters have been chosen to model the Si2p core-level on a Si(111) surface which has been exposed to hydrogen fluoride (cf. Fig. 2. from Ref. 2) and some Gaussian noise has been added. Also shown (full lines upper figure) are the curves corresponding to the input parameters that were used for the least squares fit. The residuals generated by this set of input parameters are also shown. In the lower portion of the figure (full lines) is the output from the fitting program and the corresponding flat residual distribution. Note that the residuals are shown on the same scale as the Si2p core (the multiplicative factor is ×1).

was generated using experimental parameters from Ref. 2. The parameters describe the form of a Si2p core-level, measured with 108 eV synchrotron light, when a Si(111) surface is exposed to hydrogen fluoride. The input parameters to the least-squares fit were generated by increasing the $Si2p_{3/2}$ model parameters (intensity and widths) by 1% and decreasing the $Si2p_{1/2}$ parameters by the same amount (Fig. 1). In the least-squares minimization, the Voigt function was evaluated using the analytical approximation and also by numerically integrating the convolution integral. The time taken to do the latter depends upon the point at which the convolution integral is truncated and we used $2.5\gamma_G \approx 5.9\sigma$ in this comparison. The results are presented in Table 2. The fit was performed with different point densities to show that the time taken to achieve convergence scales linearly with the number of points (ignoring the round off error) when the approximation is used. As expected, the time to convergence increases geometrically when the convolution integral is evaluated numerically. Increasing the number of Voigts has a similar effect.

Table 2
Efficiency of the analytical Voigt function approximation compared with the numerical evaluation of the convolution integral in a fit of a synthetic Si2p core-level spectrum (see text)

Number of points	Approximation[a]	Convolution
100	1	57
200	2	228
300	4	459
400	5	773

[a] Times are rounded up to the nearest second.

4. Accuracy

The accuracy of the approximation has been discussed in the source paper [11]. However, for completeness, we have calculated the maximum absolute error for a simple case. This was done by convoluting a unit width Lorentzian of unit height with a Gaussian of unit area. The convolution was performed for 5 different Gaussian widths which were chosen so that the ratio $\gamma_L/\gamma_G = 0.1, 0.3, 1.0, 3.0$ and 10. The maximum absolute errors in the range −10 to 10 are presented in Table 3. This also allows us to make a direct comparison between the four generalized Lorentzian approximations [11] and the linear sum of a Gaussian and a Lorentzian [1] for $\gamma_L/\gamma_G = 1.0$. In this case, the former is accurate to within -3.65×10^{-4}, while the latter is accurate

Table 3
Accuracy of the Voigt approximation, measured by convoluting a unit width Lorentzian of unit height with a Gaussian of unit area for five different Gaussian widths (see text)

γ_L/γ_G	Absolute error
10	-7.94×10^{-5}
3.0	-1.89×10^{-4}
1.0	-3.65×10^{-4}
0.3	-2.94×10^{-4}
0.1	$+6.29 \times 10^{-5}$

to within about -6×10^{-3}. Furthermore, it is apparent from Table 3 that the four Lorentzian approximation reproduces the Gaussian limit, $\gamma_L/\gamma_G = 0.1$, very well.

5. Surface states on gallium arsenide

To illustrate the efficiency of the approximation in a different setting, we have used our implementation of the approximation to perform lineshape analysis on an angle-resolved valence band photoemission energy distribution curve taken from GaAs(110). The main reason for doing this is to obtain precise estimates of the photoemission peak positions, which in an angle-resolved experiment translate directly into precise estimates of the initial state bands.

For many III–V semiconductors, the photoemission lineshapes appear to be highly symmetric, although there is no a priori justification for this. Consequently, it is quite common for experimenters to fit symmetric Gaussian, Lorentzian or Voigt functions to valence band spectra to extract peak positions [4,16]. Although the photoemission lines may indeed be weakly asymmetric, lineshape analysis with symmetric lines is still to be preferred over the assignment of peak positions to maxima in the energy distribution curves. The problems associated with the latter are well known and do not have to be documented here. However, it is only possible to perform detailed studies of valence band lineshapes when the photoemission lines do not strongly overlap. This occurs, for example, when the initial state is a two-dimensional

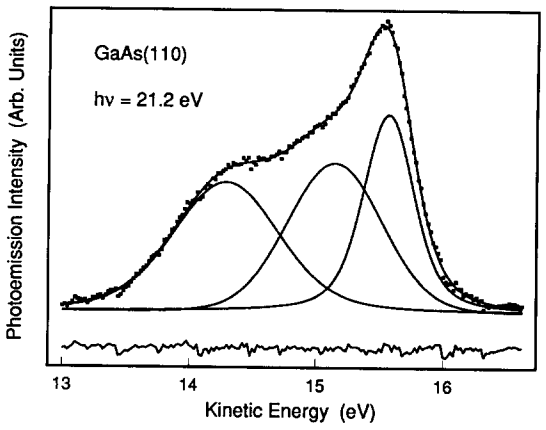

Fig. 2. An angle-resolved, valence band photoemission spectrum (dots) collected from the GaAs(110) surface with unpolarized $\hbar\omega = 21.2$ eV light. The uppermost state is probed in the neighborhood of the $\overline{X}'$ point of the surface Brillouin zone. Also shown are the results of fitting three Voigts to the energy distribution curve. The secondary electron background has been removed for clarity. The residual distribution is also shown. Notice that the residuals have not been rescaled relative to the raw data. The multiplicative factor is $\times 1$.

surface state which is not, by definition, in resonance with the bulk continuum. Therefore, the conditions that produce a clearly resolved feature in the photoemission spectrum may also be the conditions under which we would expect the smallest asymmetry in the line profile. In fact, if the asymmetry could be measured and quantified it should, in principle, be possible to extract information about the quasiparticle self energy. At present, this is an interesting possibility that is far beyond the scope of this paper.

In Fig. 2 we show a valence band photoemission curve, collected from the GaAs(110) surface with He I radiation ($\hbar\omega = 21.2$ eV), in which the uppermost surface state (A_5) is probed near the $\overline{X}'$ symmetry point of the surface Brillouin zone. Although the energy distribution curve has only one well defined maximum, three Voigt functions are required to model this energy distribution curve. Both two and three component fits produce non-uniform residual distributions which exhibit large systematic excursions from zero. The uppermost state (A_5) is approximately half the width of the other two states and the energy separation of the upper two states is about 0.42 eV. This is

reassuring, because band structure calculations [17] predict the existence of two closely spaced ($\Delta E \approx 0.3$ eV) surface bands in this region of the surface reciprocal zone. The peaks at 15.15 and 15.57 eV can be assigned to transitions from the A_4 and A_5 surface bands respectively, and this type of analysis allows the dispersion of the A_4 state to be studied in detail. At the $\overline{X}'$ point the A_5 state is split off from the bulk bands whereas the A_4 state overlaps the bulk continuum and it is technically a surface resonance [17]. It is interesting to note that the linewidth of the A_5 surface state is considerably narrower than the linewidth of the A_4 surface resonance suggesting that the lifetime of the A_5 surface state (valence hole) is almost two times larger than the lifetime of the A_4 surface resonance.

We fitted the valence band photoemission energy distribution curve with three Voigt functions using the approximation and by numerically evaluating the convolution integral. The curve contained 182 points and the fit took 22 s using the approximation and 7502 s (a factor of 341) when the Voigt functions were numerically evaluated, clearly demonstrating the advantage of using the numerical approximation to determine the peak positions.

6. Conclusions

It has been demonstrated that an analytical approximation to the Voigt function can readily be employed in lineshape analysis without significant loss of numerical accuracy. We have presented two ANSI C implementations of this approximation that can easily be incorporated in a non-linear lineshape analysis programme, such as *mrqmin* from Numerical Recipes in C [14]. The efficiency of the analytical approximation brings photoemission lineshape analysis within the domain of desktop computers.

Acknowledgments

This research was supported by the Natural Sciences and Engineering Research Council of Canada and the Advisory Research Committee of Queen's University, Canada. We gratefully acknowledge discussions with D.G. Rancourt, and we thank the referee for several constructive comments.

References

[1] G.K. Wertheim and S.B. Dicenzo, J. Electron Spectrosc. Relat. Phenom., 37 (1985) 57.
[2] F.J. Himpsel, F.R. McFeely, J.F. Morar, A. Taleb-Ibrahimi and J.A. Yarmoff, in M. Campagna and R. Rosei (Eds.), Proceedings of the 1988 Enrico Fermi School of Photoemission and Absorption Spectroscopy of Solids and Interfaces with Synchrotron Radiation, North Holland, Amsterdam, 1989, p. 203.
[3] S. Doniach and M. Šunjić, J. Phys. C, 3 (1970) 285.
[4] J. Fraxedas, J. Trodahl, S. Gopalan, L. Ley and M. Cardona, Phys. Rev. B, 41 (1990) 10068.
[5] R.A. Bartynski, E. Jensen, T. Gustafsson and E.W. Plummer, Phys. Rev. B, 32 (1985) 1921.
[6] G.A. Benesh and J.E. Inglesfield, J. Phys. C, 19 (1986) L543.
[7] W. Voigt, Sitzungsber. Math. Naturwiss. Kl. Bayer. Akad. Wiss. München, (1912) 603.
[8] G.K. Wertheim, M.A. Butler, K.W. West and D.N.E. Buchanan, Rev. Sci. Instrum., 45 (1974) 11, 1369.
[9] J.J. Joyce, M. Del Giudice and J.H. Weaver, J. Electron Spectrosc. Relat. Phenom., 49 (1989) 31.
[10] P. Martin and J. Puerta, Appl. Opt., 20 (1981) 259.
[11] J. Puerta and P. Martin, Appl. Opt., 20 (1981) 3923.
[12] D.G. Rancourt, Nucl. Instrum. Methods B, 44 (1989) 199–210.
[13] D.G. Rancourt and J.Y. Ping, Nucl. Instrum. Methods B, 58 (1991) 85–97.
[14] W.H. Press, B.P. Flannery, S.A. Teukolsky and W.T. Vetterling, Numerical Recipes in C, 1st edn., Cambridge University Press, 1988.
[15] D.W. Marquardt, J. Soc. Ind. Appl. Math., 11 (1963) 431.
[16] D.M. Swanston, A.B. McLean, D.N. McIlroy, D. Heskett, R. Ludeke, H. Munekata and M. Prietsch, Can. J. Phys., 70 (1992) 1099.
[17] J.R. Chelikowsky and M.L. Cohen, Phys. Rev. B, 20 (1979) 10, 4150.
[18] W.H. Press, B.P. Flannery, S.A. Teukolsky and W.T. Vetterling, Numerical Recipes in C, Example Book, 1st edn. Cambridge University Press, 1988.

Appendix A: The Voigt function

The ANSI C function *vs* evaluates the magnitude of the Voigt photoemission lineshape at x using the

analytical approximation described in the text. The function takes as arguments the Lorentzian amplitude *a_L*, the position of the Voigt function *pos*, the Lorentzian FWHM *gamma_L* and the Gaussian FWHM *gamma_G*. The naming convention follows the conventions adopted in the main text.

```
#define SQR(a)((a)*(a))

float
vs(float a_L,float pos,float gamma_L,float gamma_G,float x)
{
  unsigned i;
  float A[4],B[4],C[4],D[4],V=0;
  static float sqrtln2=0.832554611;
  static float sqrtpi=1.772453851;
  float X=(x-pos)*2*sqrtln2/gamma_G;
  float Y=gamma_L*sqrtln2/gamma_G;


  A[0]=-1.2150; B[0]= 1.2359;
  A[1]=-1.3509; B[1]= 0.3786;
  A[2]=-1.2150; B[2]=-1.2359;
  A[3]=-1.3509; B[3]=-0.3786;
  C[0]=-0.3085; D[0]= 0.0210;
  C[1]= 0.5906; D[1]=-1.1858;
  C[2]=-0.3085; D[2]=-0.0210;
  C[3]= 0.5906; D[3]= 1.1858;

  for(i=0;i<=3;i++)
    V+=(C[i]*(Y-A[i])+D[i]*(X-B[i]))/(SQR(Y-A[i])+SQR(X-B[i]));

  return(gamma_L*a_L*sqrtpi*sqrtln2/gamma_G)*V;
}

#undef SQR
```

Appendix B: The Voigt function and analytical parameter derivatives

The ANSI C function *VS* evaluates the magnitude of the Voigt photoemission lineshape and the four parameter derivatives using the analytical approximation described in the text. *VS* can be called directly from *mrqmin*, an implementation of the Levenberq–Marquardt non-linear least-squares minimization method [14]. The parameters have been named following the conventions used in Ref. 14. To summarize, x is the point at which the magnitude of the Voigt function is to be evaluated, $a[1 \ldots m]$ is a one-dimensional matrix of type float that contains the Voigt parameters (in the order Lorentzian amplitude, position, Lorentzian FWHM, Gaussian FWHM...), $dyda[1 \ldots m]$ is a one-dimensional matrix of type float which contains the parameter derivatives, y is a float pointer which is set to the magnitude of the Voigt function at x and m is the number of parameters. For a single Voigt $m = 4$, for two Voigts $m = 8$, etc. The reader is recommended to consult Ref. 18 for information about how to call *VS* from *mrqmin*.

```
#define SQR(a) ((a)*(a))

void
VS(float x,float* a,float* y,float* dyda,int m)
{
  unsigned i,j;
  static float sqrtln2=0.832554611;
  static float sqrtpi=1.772453851;
  float A[4],B[4],C[4],D[4],alpha[4],beta[4];
  float dVdx=0.0,dVdy=0.0,V=0.0,X,Y,constant;

  A[0]=-1.2150; B[0]= 1.2359; C[0]=-0.3085; D[0]= 0.0210;
  A[1]=-1.3509; B[1]= 0.3786; C[1]= 0.5906; D[1]=-1.1858;
  A[2]=-1.2150; B[2]=-1.2359; C[2]=-0.3085; D[2]=-0.0210;
  A[3]=-1.3509; B[3]=-0.3786; C[3]= 0.5906; D[3]= 1.1858;

  *y=0.0;
  for(i=1;i<=m-1;i+=4)
  {
    X=(x-a[i+1])*2*sqrtln2/a[i+3];
    Y=a[i+2]*sqrtln2/a[i+3];
    constant=a[i+2]*a[i]*sqrtpi*sqrtln2/a[i+3];

    for(j=0;j<=3;j++)
    {
      alpha[j]=C[j]*(Y-A[j])+D[j]*(X-B[j]);
      beta[j]=SQR(Y-A[j])+SQR(X-B[j]);
      V+=alpha[j]/beta[j];
      dVdx+=D[j]/beta[j]-2.0*(X-B[j])*alpha[j]/SQR(beta[j]);
      dVdy+=C[j]/beta[j]-2.0*(Y-A[j])*alpha[j]/SQR(beta[j]);
    }

    *y+=constant*V;
    dyda[i]=constant*V/a[i];
    dyda[i+1]=-constant*dVdx*2*sqrtln2/a[i+3];
    dyda[i+2]=constant*(V/a[i+2]+dVdy*sqrtln2/a[i+3]);
    dyda[i+3]=-constant*(V+(sqrtln2/a[i+3])*
              (2.0*(x-a[i+1])*dVdx+a[i+2]*dVdy))/a[i+3];
  }
}
#undef SQR
```